Applied Surface Science 469 (2019) 804–810

Contents lists available at ScienceDirect

Applied Surface Science

journal homepage: www.elsevier.com/locate/apsusc

Full Length Article

A kinetic study of ZnO atomic layer deposition: Effects of surface hydroxyl concentration and steric hindrance

Sungjoon Kim[1], Sunyoung Lee[1], So-Yeon Ham, Dong-Hyun Ko, Seokhee Shin, Zhenyu Jin, Yo-Sep Min*

Department of Chemical Engineering, Konkuk University, 120 Neungdong-Ro, Gwangjin-Gu, Seoul 05029, South Korea

ARTICLE INFO

Keywords:
Atomic layer deposition
ZnO
Kinetic study

ABSTRACT

We present a kinetic model for the reaction of diethylzinc (DEZ) adsorption in atomic layer deposition (ALD) of ZnO from DEZ and water. The proposed model has been verified by comparing kinetic experimental data to the prediction of the model in the temperature range of 60–200 °C. In this model, DEZ molecules are molecularly adsorbed on the hydroxyl-terminated surface in the first elementary reaction. Then the molecularly-adsorbed DEZs either desorb from the surface, or undergo an irreversible ligand exchange reaction and form mono-ethylzinc (MEZ)-terminated surface by liberating ethane molecules. According to the integrated rate law of the model, as the exposure time of DEZ increases, the growth per cycle (*gpc*) of ALD, i.e., the thickness increment per cycle, rapidly increases and then saturates showing the self-limiting growth behavior. The required DEZ exposure time to reach the saturated *gpc* value is shortened when the chemical equilibrium between the molecular adsorption and desorption shifts toward the adsorption, as this leads to higher effective rate constant in the overall mechanism of the DEZ adsorption. Although the saturated *gpc* value is primarily governed by the hydroxyl concentration on the ZnO surface, it is also heavily influenced by the steric hindrance due to the bulkiness of the ethyl ligands. We have determined that the critical temperature at which the steric hindrance disappears is around 150–200 °C, by investigating the variation of the hydroxyl concentration with temperature. At temperatures lower than 150 °C, we have observed that the saturated *gpc* value is governed by the steric hindrance rather than the hydroxyl concentration. However, the saturated *gpc* value at 200 °C has been achieved purely by the hydroxyl concentration. In other words, all hydroxyl groups at 200 °C have been consumed and saturated by the MEZ molecules of which the steric hindrance-free concentration has been evaluated to be ~7.1 /nm^2. In addition, the effective activation energy was estimated to be ~8.50 kJ/mol by using the effective rate constants of all temperatures investigated.

1. Introduction

Recently, atomic layer deposition (ALD) method has been widely utilized to grow thin films or nano-materials for various applications such as electronic devices, solar cells, and catalysis due to its precise controllability in atomic scale [1]. ALD is a thin film deposition method in vacuum and a modified version of chemical vapor deposition (CVD). In the CVD method, two (or more) precursor gases are simultaneously supplied to a substrate at a high temperature to chemically deposit a thin film, accompanying thermal decomposition of precursors. However, In the ALD, the two precursor gases are alternately pulsed onto the substrate, and each pulse of precursors are separated by purging with inert gas, in order to avoid the encounter and thermal decomposition of both precursors. Consequently, the thin film growth in the ALD is accomplished by chemical adsorption of each precursor via two self-limiting half-reactions. After adsorption sites in the surface are saturated with one type of precursor molecules, the chemical reaction is terminated showing self-limiting growth behavior. Additional precursor molecules of the same type do not adsorb onto the surface, since all available sites have been consumed. This self-limiting behavior enables ALD to finely control the film growth in angstrom-scale. In addition, the surface species formed by the chemical adsorption plays a role of adsorption sites for the chemical adsorption of the other precursor in the next half-reaction. Therefore, by repeating the ALD cycle which consists of the first half-reaction, purge, the second half-reaction and purge, the thickness of the thin film increases with the number of ALD cycles.

* Corresponding author.
E-mail address: ysmin@konkuk.ac.kr (Y.-S. Min).
[1] These authors (S.K. and S.L.) equally contributed to this work.

https://doi.org/10.1016/j.apsusc.2018.11.064
Received 12 October 2018; Received in revised form 7 November 2018; Accepted 8 November 2018
Available online 09 November 2018
0169-4332/

Among ALD processes of various materials, ZnO has been extensively studied due to the existence of near-ideal precursors, i.e., diethylzinc and water for zinc and oxygen, respectively. ZnO is a semiconducting material with a wide band gap of 3.37 eV. Its useful properties such as tunable conductivity and transparency have led to various ZnO applications, such as passivation layers in solar cells, [2,3] channel layers in thin film transistors, [4–6] and photoelectrochemical catalysis. [7–10] Piezoelectricity of ZnO also allows ZnO thin films to be used in sensor applications to detect changes in pressure and gas composition [11,12]. Combination with unique materials such as graphene has also been studied in recent years [13] In these applications of ZnO thin films, ALD is one of the favored deposition methods, due to its ability to comply with the current market's stringent demands for device fabrication [14,15].

Understanding the ALD mechanism is important because it allows the user to finely tune the ALD process, which in turn leads to optimal properties of the deposited films. Knowledge regarding the energetics and kinetics of ALD reactions would also help optimize the ALD processes, by reducing the amount of wasted precursors and shortening the deposition process. Despite the intensive investigations, [16–18] the mechanisms of many ALD reactions including the ZnO ALD process are still under debate due to the complicated nature of the reaction environment [19–21]. In an ideal scenario of ALD, one ALD cycle would deposit a monolayer of the target material. However, practical factors such as steric hindrance exerted from ligands of precursors and/or the lack of surface adsorption sites may prevent the realization of the monolayer growth per cycle (*gpc*). Such deviations complicate the study of kinetics and mechanisms.

In an effort to investigate the complicated mechanisms, theoretical approaches which are based on first principles have been used [20,22,23] Density functional theory (DFT) relies on the computation of atomic interactions and bonds to calculate the energies and plausibility of given chemical reactions. Despite its usefulness, the inherent simplifications and assumptions (such as crystallinity, temperatures, etc.) needed to achieve the calculations can yield over- or under-estimated predictions which differ from actual experimental results. Thus, real experimental data are required to confirm that the obtained calculations are valid.

Puurunen reported a theoretical close packing model for *gpc* in ALD where she assumes that the steric hindrance between precursor molecules determines the *gpc* of ALD reactions [24]. The model uses the bulkiness of precursor ligands to calculate the area each precursor takes up on the surface. The area taken up by one ligand is then used to determine the number of precursor molecules able to adsorb on the surface. This model explains the decreasing *gpc* at high temperatures with the decrease in surface adsorption sites. However, it neglects the effect of a change in temperature when the *gpc* value is determined by the steric hindrance. In practice, the *gpc* value often increases in this region as the temperature increases, since the number of molecules having enough energy to overcome the energy barrier of adsorption is also increased.

Here, we propose a simple kinetic model for the adsorption of diethylzinc (DEZ) on the surface of ZnO. In the proposed mechanism, the reversible molecular DEZ adsorption step exists prior to the irreversible chemisorption of DEZ. The integrated rate law from the model is well matched with the kinetic data of the pre-saturation regions in the self-limiting adsorption of DEZ. Among various factors such as the equilibrium between adsorption and desorption of DEZ, surface hydroxyl concentration, and steric hindrance, critical factors which govern the *gpc* value are investigated in detail.

2. Experimental

ZnO films were deposited on boron-doped *p*-type Si (1 0 0) wafers with a resistivity of 10.0 Ω cm (LG Siltron, Inc., CASRN: 7440-21-3) in a laminar flow type reactor (ATOMIC-CLASSIC, CN1 Co., Ltd.) by ALD. DEZ (Nuri Tech Co., Ltd., CASRN: 557-20-0, 99.9999%) and deionized water (CASRN: 7732-18-5, 18 M-Ohm) were used as a precursor of zinc and oxygen, respectively. In order to reduce the dose of DEZ, an orifice with a diameter of 300μm was installed at the outlet of the precursor canister. The usage of the orifice extends the exposure time of DEZ required to reach surface saturation, enabling the investigation of the pre-saturation regions during DEZ adsorption. Before and after installing the orifice, the DEZ dose was decreased from $\sim 9.4 \times 10^{-5}$ mol/s to $\sim 8.4 \times 10^{-6}$ mol/s. To focus on the kinetics of DEZ adsorption, the water dose ($\sim 1.0 \times 10^{-4}$ mol/s) was held constant and in excess for all kinetic experiments. Both precursors were vaporized at room temperature without any carrier gas or external heating devices. The gas lines were maintained at 100 °C to prevent precursors from condensing before reaching the reaction chamber. The ALD sequence consisted of DEZ exposure - purge (10 s) - water exposure (1 s) – purge (10 s) where each pulse time was controlled by solenoid valves. The purging steps with 400 SCCM of nitrogen (Daedong Seongdong Oxygen, CASRN: 7727-37-9, 99.999%) followed each precursor exposure to remove all excess precursors and reaction byproducts existing in the gas phase. The deposition temperature was varied from 60 to 200 °C which was calibrated with a thermocouple-implanted silicon wafer under N_2 atmosphere of 1 torr.

Prior to the ALD process, the thickness of native oxide of the silicon wafer was measured by a spectroscopic ellipsometer (SE, MG-1000, Nano-View Co., LTD.), and it was used as the thickness of the native oxide in the structure model of ZnO/SiO_2/Si for measuring the thickness of the ZnO layer. Fig. 1 shows the kinetic data of the DEZ adsorption reaction (i.e., the thickness variation of ZnO as a function of DEZ exposure time) obtained at various ALD temperatures (60, 80, 100, 125, 150, and 200 °C).

3. Results and discussion

3.1. Kinetic model for DEZ adsorption

The ALD of ZnO can be broken down to two half-reactions which are responsible for the deposition of zinc and oxygen atoms, respectively [19,25]. The first (Eq. (1)) and second (Eq. (2)) half-reactions during DEZ and water pulses are respectively represented by

$$\text{⊩OH} + \text{Zn}(\text{CH}_2\text{CH}_3)_2(\text{g}) \rightarrow \text{⊩OZn}(\text{CH}_2\text{CH}_3) + \text{C}_2\text{H}_6\ (\text{g}) \quad (1)$$

$$\text{⊩Zn}(\text{CH}_2\text{CH}_3) + \text{H}_2\text{O}\ (\text{g}) \rightarrow \text{⊩ZnOH} + \text{C}_2\text{H}_6\ (\text{g}) \quad (2)$$

where the symbol ⊩ denotes surface species. The surface hydroxyls play a role of the adsorption sites for DEZ. The monoehtylzinc (MEZ) formed in the first half-reaction reacts with water vapor to recover the surface hydroxyls in the second half-reaction. Among the two half-reactions, we

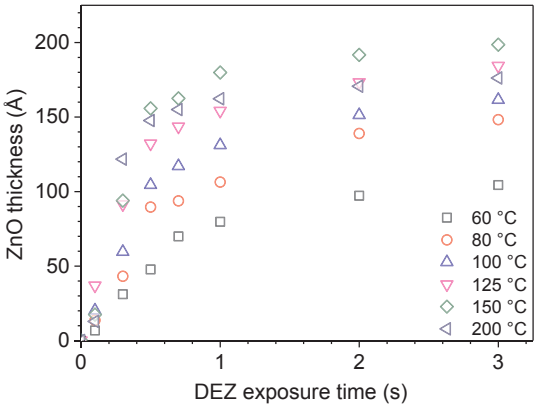

Fig. 1. ZnO thickness variations as a function of DEZ exposure time at various deposition temperatures. Each point represents the thickness resulting from 100 ALD cycles.

will focus on the adsorption reaction of DEZ, because the kinetic data (i.e., *gpc* values) of ALD are generally governed by the adsorption of the bulkier precursor, due to its steric hindrance [24].

We propose a mechanism of the first half-reaction for the DEZ adsorption which consists of three elementary reactions as listed below (Eqs. (3)–(5))

$$\text{⊩OH} + \text{DEZ} \xrightarrow{k_a} \text{⊩OH:DEZ} \tag{3}$$

$$\text{⊩OH: DEZ} \xrightarrow{k_d} \text{⊩OH} + \text{DEZ} \tag{4}$$

$$\text{⊩OH: DEZ} \xrightarrow{k_b} \text{⊩OZn}(CH_2CH_3) + C_2H_6 \tag{5}$$

where the symbol : denotes long-range interaction by molecular adsorption, and k_a, k_d and k_b are the rate constants of each elementary reaction. Note that the steric hindrance of the surface species is not considered in this mechanism for simplicity (see the following sections for the steric hindrance).

According to the DFT calculations by Weckman et al., DEZ molecules form a pre-adsorbed state with the surface hydroxyl group [23]. The adsorption energy of this interaction is around − 0.7 to − 0.5eV, suggesting that the nature of the adsorption is not chemical, but rather a weak molecular interaction (Eq. (3)). Since the molecular adsorption is reversible, the molecularly-adsorbed DEZs either desorb from the surface (Eq. (4)) or undergo the ligand exchange reaction (Eq. (5)) to chemically adsorb on the surface. The ligand exchange reaction is considered irreversible due to two reasons. First, during the ALD process, the liberated ethane gas is rapidly purged from the reactor, eliminating the possibility of a reverse reaction. Second, according to the DFT calculation [23] the energy barrier for the reverse reaction (1.16 eV) is much larger than that (0.24 eV) of the ligand exchange reaction. The large energy barrier eliminates the possibility of the reverse reaction, even in the presence of nearby ethane.

For simplicity, the proposed mechanism is rewritten with Roman and Greek letters for gas phase molecules and surface species, respectively.

$$\alpha + \text{D} \xrightarrow{k_a} \beta \tag{3a}$$

$$\beta \xrightarrow{k_d} \alpha + \text{D} \tag{4a}$$

$$\beta \xrightarrow{k_b} \gamma + \text{E} \tag{5a}$$

where α, β, γ, D and E represent the surface hydroxyls, molecularly-adsorbed DEZ, chemically-adsorbed MEZ, gaseous DEZ, and ethane, respectively. The proposed reaction pathway is simply summarized as below

$$\alpha + \text{D} \rightleftarrows \beta \rightarrow \gamma + \text{E} \tag{6}$$

According to the proposed mechanism, the rate of change in the concentration of the molecularly-adsorbed DEZ (β) is given by

$$\frac{d[\beta]}{dt} = k_a[\alpha]P_{DEZ} - k_d[\beta] - k_b[\beta] \tag{7}$$

where the symbols in square brackets indicate each concentration of surface species of which the dimension is the number of the surface species per unit area. P_{DEZ} is the vapor pressure of DEZ and is around 0.14–0.18 torr in our kinetic experiments during the exposure of DEZ with the orifice of 300 μm in diameter. We may assume that the rate of change in [β] is negligibly small after an induction period (an interval during which [β] rises from zero to a steady-state concentration) and before the complete consumption of the surface hydroxyls (α). By using the quasi-steady state approximation at the intermediate stage of the progress of the reaction except for the initial and final stages, the concentration of β is expressed as

$$[\beta] = \frac{k_a[\alpha]P_{DEZ}}{k_b + k_d} \tag{8}$$

By setting a pressure constant (Π) as

$$\Pi = \frac{k_b + k_d}{k_a} \tag{9}$$

and

$$[\beta] = \frac{[\alpha]P_{DEZ}}{\Pi} \tag{10}$$

Note that the pressure constant Π is a function of temperature, and the dimension of Π is 'pressure', because the units of the rate constants are s^{-1} for both k_b and k_d, and $s^{-1}\cdot torr^{-1}$ for k_a. Furthermore, because the initial concentration ($[\alpha]_0$) of the surface hydroxyls should be the sum of [α], [β] and [γ], and P_{DEZ} is approximately equal to the initial vapor pressure of DEZ ($P_{0,DEZ}$) owing to its continuous supply for the DEZ exposure, [β] can be rewritten as

$$[\beta] = \frac{P_{0,DEZ}([\alpha]_0 - [\gamma])}{\Pi + P_{0,DEZ}} \tag{11}$$

Consequently, the rate law of the first-half reaction is expressed as

$$\frac{d[\gamma]}{dt} = k_b[\beta] = \frac{k_b P_{0,DEZ}([\alpha]_0 - [\gamma])}{\Pi + P_{0,DEZ}} \tag{12}$$

and, by integrating Eq. (12),

$$[\gamma] = [\alpha]_0\left(1 - \exp\left(-\frac{k_b P_{0,DEZ}}{\Pi + P_{0,DEZ}}t\right)\right) \tag{13}$$

where t is the exposure time of DEZ. The integrated rate law (Eq. (13)) implies that all initial adsorption sites (α) are completely occupied by MEZ at an infinitely long exposure time (i.e., $[\gamma] = [\alpha]_0$ at $t = \infty$). Thus, the first term ($[\alpha]_0$) of Eq. (13) can be interpreted as the concentration of the adsorption sites which can be potentially converted to the MEZ-adsorbed sites under the assumption of no steric hindrance. The second term represents the concentration of the adsorption sites which is not occupied by MEZ and remains in the form of α or β at an exposure time t. Therefore, if there is no steric hindrance between the adsorbed molecules, the [γ] value should be primarily governed by the $[\alpha]_0$ value. However, if steric hindrance does exist, the [γ] value will secondarily be decided by the steric hindrance. Thus, the importance of the degree of steric hindrance in DEZ adsorption becomes apparent.

In addition, the second term is a decaying exponential function of which the decaying rate is determined by k_b, $P_{0,DEZ}$, and Π. Depending on the values of Π and $P_{0,DEZ}$, the integrated rate law can be approximated as

$$[\gamma] \cong [\alpha]_0\left(1 - \exp\left(-\frac{k_b P_{0,DEZ}}{\Pi}t\right)\right) \text{ if } \Pi \gg P_{0,DEZ} \tag{14}$$

and

$$[\gamma] \cong [\alpha]_0(1 - \exp(-k_b t)) \text{ if } \Pi \ll P_{0,DEZ} \tag{15}$$

Consequently, the latter ($\Pi \ll P_{0,DEZ}$) may show a more rapid saturation of [γ] compared to the former ($\Pi \gg P_{0,DEZ}$). According to Eq. (9), for the pressure constant to become smaller, the rate constant of the molecular adsorption (k_a) should be higher than that of the ligand exchange reaction (k_b) and/or that of the molecular desorption (k_d). Eq. (13) can be further simplified by setting k_{eff} as

$$k_{eff} = \frac{k_b P_{0,DEZ}}{\Pi + P_{0,DEZ}} \tag{16}$$

and

$$[\gamma] = [\alpha]_0(1 - \exp(-k_{eff} t)) \tag{17}$$

where k_{eff} can be interpreted as the effective rate constant of the overall first-half reaction.

3.2. Application of the proposed kinetic model

As shown in Fig. 1, our kinetic data are plotted as thicknesses grown for 100 cycles at various temperatures against the DEZ exposure time. To verify the kinetic data with the proposed model, the growth per cycle (*gpc*), which is defined as thickness increment per cycle at DEZ exposure time *t*, can related with [γ] as below

$$gpc = \frac{M}{\rho N_A}[\gamma] \tag{18}$$

where M, ρ, and N_A represent the molar mass and density of ZnO, and the Avogadro's number, respectively [24,26]. It is reported that the density of ZnO grown by ALD using DEZ and water is around 5.4 g/cm^3 [27]. Combining Eqs. (17) and (18), the integrated rate law can be rewritten as

$$gpc = \frac{[\alpha]_0 M}{\rho N_A}(1 - \exp(-k_{eff}\, t)) \tag{19}$$

and *gpc* is a function of the DEZ exposure time and saturates at a long exposure time. If there is no steric hindrance as assumed in this model, the saturated *gpc* (gpc_{sat}) is determined by the initial concentration of surface hydroxyls ($gpc_{sat} = [\alpha]_0 M/\rho N_A$).

Morishige, et al. performed a thermal desorption study of water molecules which occurs from molecularly-adsorbed H_2O or chemically-adsorbed surface hydroxyl on ZnO [28]. However, they did not quantify the surface hydroxyl concentration (i.e., OH/nm^2) remaining on the surface, but instead determined the number of hydroxyl groups per 1 nm^2 which were removed from the ZnO surface by the thermal desorption. The total sum of hydroxyls removed during heating ZnO samples from 40 to 400 °C was around 11–12 OH/nm^2. By integrating their thermal desorption spectra in a temperature range of interest and subsequently subtracting the number of hydroxyls removed in the temperature range from the total number of hydroxyls, we extracted the surface hydroxyl concentration (i.e., $[\alpha]_0$) at specific temperatures as shown in Fig. 2 (see Fig. S2 for the extended data in a wider temperature range).

Using the surface hydroxyl concentrations of Fig. 2, the saturation behavior of [γ] can be predicted by the proposed model (Eq. (17)), if the value of k_{eff} is known at the temperature of interest. In Fig. 3, the theoretical and experimental values of [γ] are plotted against the DEZ exposure time (*vide infra* for the determination of the k_{eff} values). The proposed model well depicts the saturation behavior of [γ] at 200 °C as shown in Fig. 3a. It reveals that there is no steric hindrance at 200 °C. However, there is a significant difference between the experimental and theoretical [γ] values at 100 °C. The discrepancy originates from the steric hindrance which is neglected in the proposed model. This discrepancy becomes more severe as the growth temperature decreases (see Fig. S3). This is due to the higher $[\alpha]_0$ values at lower temperatures.

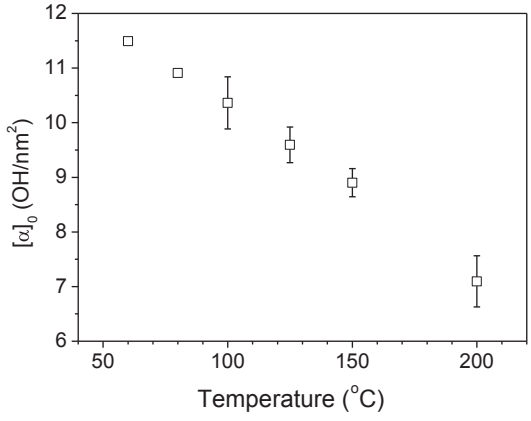

Fig. 2. Surface hydroxyl concentration on ZnO as a function of temperature. The data used to plot this figure has been extracted from the thermal desorption spectra of Ref. [28].

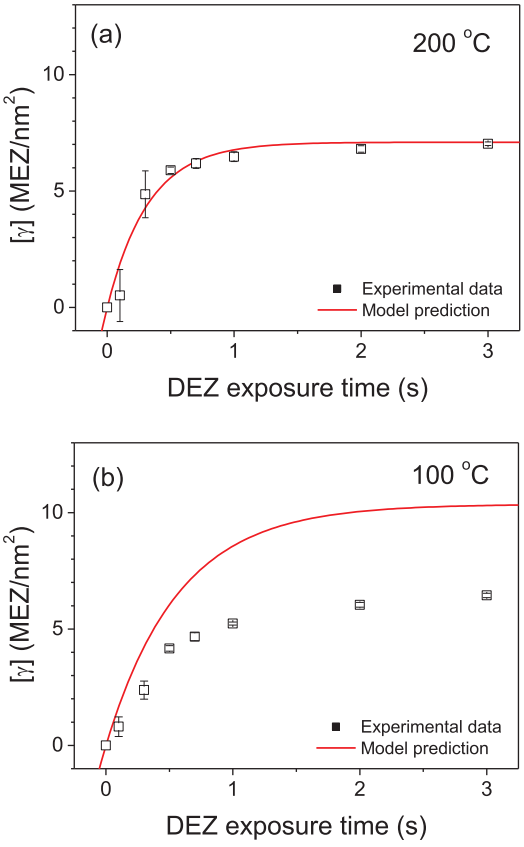

Fig. 3. Comparison of saturation behaviors of [γ] at 100 °C (a) and 200 °C (b) against DEZ exposure time. The solid lines were calculated from Eq. (17): k_{eff} = 3.08/s and $[\alpha]_0$ = 7.1/nm^2 at 200 °C; k_{eff} = 1.75/s and $[\alpha]_0$ = 10.4/nm^2 at 100 °C. The experimental data of [γ] were obtained from the *gpc* values by using Eq. (18).

If steric hindrance exists, the maximum number of adsorbed MEZ will not be decided by the initial concentration of surface hydroxyls. Although unoccupied hydroxyl sites exist on the surface, the maximum number of adsorbed MEZ will be decided by the degree of steric hindrance. Thus, the saturation of [γ] may occur at an earlier exposure time (t_s') with a lower gpc_s' than those (t_{sat} and gpc_{sat}) predicted by the model. However, even if steric hindrance persists, since the adsorption of DEZ may follow the proposed pathway and the measured *gpc* cannot exceed the gpc_s' value, we can express the saturation behavior in the normalized form with gpc_s' as below

$$\frac{gpc}{gpc_s'} = \frac{1 - e^{-k_{eff}\, t}}{1 - e^{-k_{eff}\, t_s'}} \tag{20}$$

In our kinetic experimental data, the *gpc* nearly saturates at $t_s' = 3s$ at all temperatures as shown in Fig. 1. Therefore, using the gpc_s' value at $t_s' = 3s$, we performed a nonlinear regression of the kinetic data with Eq. (20) in order to determine the effective rate constant (k_{eff}) at each temperature. For example, from the nonlinear regression of the kinetic data at 100 °C (Fig. 4), we have obtained the effective rate constant of ~1.75/s. The other regression data at different temperatures are listed in Table 1 (see Fig. S4 for other temperatures). The regression results and experimental data are well matched at all temperatures, indicating that the adsorption of DEZ follows the proposed kinetics.

Using the effective rate constants listed in Table 1, the effective activation energy for the DEZ adsorption reaction was estimated to be 8.50 kJ/mol ± 0.67 (0.09 eV ± 0.01) from the Arrhenius plot (Fig. 5) in

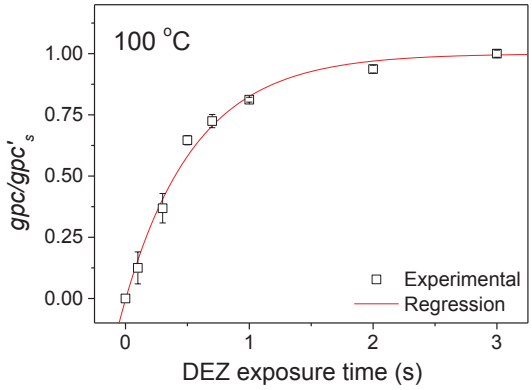

Fig. 4. Variation of $gpc/gpc_s^{'}$ against DEZ exposure time at 100 °C (see Fig. S4 for other temperatures).

Table 1
The effective rate constants and surface hydroxyl concentrations at various ALD temperatures.

Temperature [°C]	k_{eff} [s^{-1}]	Standard deviation	$[\alpha]_0$ [nm^{-2}]
60	1.30	0.08	11.5
80	1.38	0.11	10.9
100	1.75	0.09	10.4
125	2.23	0.11	9.6
150	2.36	0.22	8.9
200	3.08	0.42	7.1

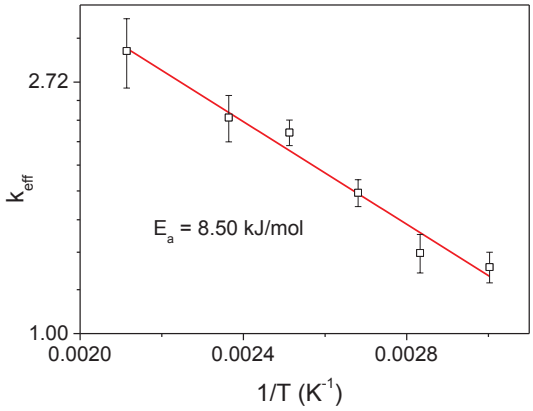

Fig. 5. Arrhenius plot of the DEZ adsorption reaction.

the temperature range of 60–200 °C. There have been several studies in which the growth per cycle data in the saturated region (i.e., $gpc_s^{'}$) were used to calculate the apparent activation energy of DEZ adsorption [19,29]. Yousfi, et al. reported the apparent activation energy of 16.7 kJ/mol in a temperature range of 50–140 °C using their in-situ quartz crystal microgravimetric data [19]. However, the $gpc_s^{'}$ data does not represent the kinetics during precursor adsorption, and only reflects the saturated number of chemically adsorbed precursor molecules at the end of the adsorption reaction. If their approach is applied to the higher temperatures where the $gpc_s^{'}$ decreases with the increase in temperature, the apparent activation energy should become negative. Indeed, Yousifi, et al. excluded the data at temperatures higher than 140 °C for their calculations. However, by using the effective rate constants obtained by our proposed model, it is possible to calculate the effective activation energy while including the data obtained at temperatures where the gpc_s decreases with the increase in temperature. (see Fig. S5. The $gpc_s^{'}$ begins to decrease at temperatures over 150 °C in ZnO ALD). In addition, the apparent activation energy obtained from the $gpc_s^{'}$ values cannot be considered as a suitable measurement of the adsorption kinetics, as it does not encompass the kinetic aspect of the reaction which can only be obtained in the pre-saturation region.

Using DFT calculation, Afshar et al. have suggested that the adsorption of DEZ on the surface of a ZnO cluster must go through a barrier of 1.35 eV [20] which is significantly larger than the effective activation energy (0.09 eV) we have obtained. Jie et al. also has reported an activation energy value of 0.67 eV for the DEZ adsorption process [22]. These two works have used the ZnO cluster model for their calculations, which could have led to the error in estimating the barrier height. Weckman et al. have reported smaller activation energies ranging from 0.23 to 0.47 eV, depending on whether there is an adsorbed DEZ next to the active site for adsorption [23]. They modeled the surface using the common slab model with periodic boundary conditions imposed, with the slab being six stoichiometric oxide layers thick. Holmqvist et al. have reported the activation energy of DEZ adsorption reaction to be 0.44 eV [30]. The last study includes experimental results which were used to calculate the energy value, but their work mostly focuses on the statistic optimization and reactor design, rather than the ALD reaction itself.

The activation energy experimentally determined from the Arrhenius plot in our study reveals that the DFT calculations using the cluster model greatly overestimate the energy barrier of the precursor adsorption step. This error is likely the result of using ZnO clusters as substrates. Clusters and bulk layers differ significantly due to the coordination number of the atoms on the surface, therefore the ZnO film surface cannot be properly represented by a cluster model [23]. Other models which use the slab or surface model also seem to overestimate the value of activation energy. This could be due to the inherent limitations of DFT calculations, as such calculations are often carried out at 0 K. In addition, while the activation energies from the DFT calculation are the energy barrier of the elementary step in which β is converted to γ, the effective activation energy from this model is the effective barrier height in the overall mechanism. Therefore, it is reasonable that the effective activation energy is smaller than those predicted by DFT calculations. However, the resulting information from DFT calculations may be useful as a reference and for comparison with experimental data.

3.3. Comments on governing factors of $gpc_s^{'}$

As mentioned in the previous section, the presence and the degree of the steric hindrance play a critical role in achieving the theoretical saturation value of *gpc*. Here we define a steric hindrance factor (δ) to describe the degree of the steric hindrance as below

$$\delta = [\gamma]_{cal} - [\gamma]_{exp} \quad (21)$$

where $[\gamma]_{cal}$ and $[\gamma]_{exp}$ are the theoretical and experimental values of [γ], respectively. Note that the δ is a function of temperature at given conditions (i.e., t and $P_{0,DEZ}$) and can be interpreted as the lost concentration of the MEZ that would have been adsorbed on the surface if there was no steric hindrance. Fig. 6 shows the variation of δ with temperature at our experimental conditions (t = 3 s and $P_{0,DEZ} \approx 0.14\ 0.18$ *torr*) which was obtained from Fig. S3. As the temperature increases, the steric hindrance factor monotonically decreases and then disappears between 150 and 200 °C. Consequently, the experimental values and the theoretical prediction of [γ] match each other well at 200 °C as shown in Fig. 3a. Furthermore, the concentration of the surface MEZ at 200 °C is equal to the surface hydroxyl concentration of ~7.1/nm^2 at the temperature (Figs. 2 and 3a), owing to the absence of steric hindrance. According to the DFT calculation by Weckman, et al., the theoretical maximum number of MEZ on the surface of ZnO is ~7.1/nm^2 due to the steric hindrance [23]. The maximum value of the DFT calculation well agrees to that of our model.

By using the integrated rate law and the steric hindrance factor, we can determine which factor is governing the $gpc_s^{'}$, at a specific ALD

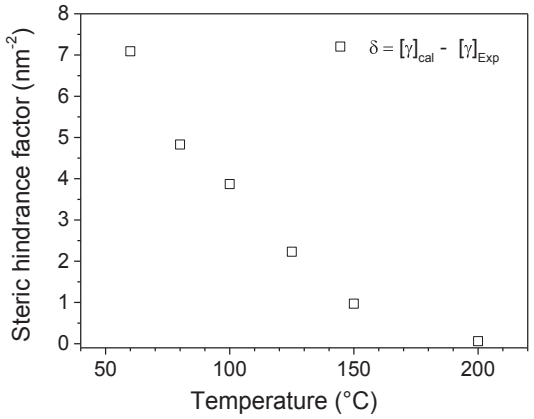

Fig. 6. Variation of steric hindrance factor with temperature. The steric hindrance factor (δ) is defined as $\delta = [\gamma]_{cal} - [\gamma]_{exp}$.

temperature. In overall, the governing factors of $gpc_s^{'}$ are the surface hydroxyl concentration and the steric hindrance. At deposition temperatures up to 150 °C, the steric hindrance determines the concentration of surface MEZ molecules. When the temperature reaches 150–200 °C, however, the surface hydroxyl concentration becomes sufficiently low that it begins to dominate the value of [γ]. The effective reaction rate constant (k_{eff}) determines how fast the film growth reaches saturation. When the rate constant becomes large, the saturation time (t_s) required to reach the surface saturation becomes shorter, as Π and k_b affect k_{eff} as mentioned previously. It should be noted that the equilibrium between the molecular adsorption and desorption of DEZ is not a determinant of $gpc_s^{'}$ but one of factors to determine the value of k_{eff}, because Π decreases as the equilibrium shifts toward adsorption. Afshar claims that the increase in deposition temperature also affects the equilibrium between adsorption and desorption of precursor molecules. He suggests that the temperatures at which the $gpc_s^{'}$ diminishes coincide with the temperatures that the adsorption of DEZ and water become thermodynamically unfavorabl [20]. However, as can be seen from the integrated rate law, the equilibrium between adsorption and desorption only affects the exposure time required to reach surface saturation, not the $gpc_s^{'}$.

In addition, since the steric hindrance is attributed to the bulkiness of the precursor ligand and is detrimental to the $gpc_s^{'}$, the usage of precursors with smaller ligands may be a viable strategy to achieve higher $gpc_s^{'}$ values. For example, using dimethylzinc (DMZ) as a Zn precursor yields higher $gpc_s^{'}$ than using DEZ at the same deposition temperature (see Fig. S5). The smaller size of the methyl ligand allows more Zn atoms to adsorb on the surface, leading to $gpc_s^{'}$ values which are closer to the monolayer thickness of ZnO [31,32]. However, the difference between the $gpc_s^{'}$ values from DEZ and DMZ becomes insignificant when the ALD temperature increases to 200 °C, as the factor determining the $gpc_s^{'}$ changes from the steric hindrance to the surface hydroxyl concentration.

4. Conclusion

A kinetic model for the DEZ adsorption reaction during ZnO ALD from DEZ and water was proposed. In this model, DEZ molecules first weakly (molecularly) adsorb on the hydroxyl-terminated surface. The molecularly-adsorbed DEZs then either desorb back into the gas phase or undergo an irreversible ligand exchange reaction by producing ethane molecules and forming MEZ-terminated surface. The proposed model has been verified by comparing the theoretical predictions with the kinetic experimental data in the temperature range of 60–200 °C. According to the integrated rate law of the model, when the exposure time of DEZ increases, the growth per cycle (*gpc*), i.e., the thickness increment per cycle, rapidly increases and then saturates, showing the self-limiting growth behavior. The DEZ exposure time required to reach the saturated *gpc* value is shortened when the chemical equilibrium between molecular adsorption and desorption shifts toward adsorption, which results in the higher effective rate constant in the overall mechanism of DEZ adsorption. The saturated *gpc* value is primarily governed by the hydroxyl concentration on the ZnO surface. However, it is also heavily influenced by the degree of steric hindrance, due to the bulkiness of the ethyl ligands. By investigating the variation of the hydroxyl concentration with temperature, we have determined that the critical temperature at which the steric hindrance disappears is between 150 and 200 °C. At temperatures lower than 150 °C, the saturated *gpc* value was governed by the steric hindrance, rather than the hydroxyl concentration. When the temperature is raised to 200 °C, however, the saturated *gpc* value was decided by the surface hydroxyl concentration. That is, all hydroxyl groups on the surface were consumed and saturated by MEZ molecules. This steric hindrance-free MEZ concentration has been evaluated to be ~7.1 /nm^2. The effective activation energy was evaluated from the effective rate constants of investigated temperatures, which was found to be ~8.50 kJ/mol.

Acknowledgements

This research was supported by the Korea Institute of Energy Technology Evaluation and Planning (KETEP: 20153030013060) and the Korea Evaluation Institute of Industrial Technology (KEIT: 10063277). This work was also partially supported by Basic Science Research Program through the National Research Foundation of Korea (NRF: 2018R1D1A1B07047768) and Samsung Research Funding & Incubation Center of Samsung Electronics, Korea (SFRC-MA1801-01).

Appendix A. Supplementary material

Supplementary data to this article can be found online at https://doi.org/10.1016/j.apsusc.2018.11.064.

References

[1] S.M. George, Atomic layer deposition: an overview, Chem. Rev. 110 (1) (2010) 111–131.
[2] J. Cao, B. Wu, R. Chen, Y. Wu, Y. Hui, B.W. Mao, N. Zheng, Efficient, hysteresis-free, and stable perovskite solar cells with ZnO as electron-transport layer: effect of surface passivation, Adv. Mater. 30 (11) (2018) 1–9.
[3] P. Das, B. Mondal, K. Mukherjee, Improved efficiency of ZnO hierarchical particle based dye sensitized solar cell by incorporating thin passivation layer in photoanode, Appl. Phys. A Mater. Sci. Process. 124 (1) (2018).
[4] S. Masuda, K. Kitamura, Y. Okumura, S. Miyatake, H. Tabata, T. Kawai, Transparent thin film transistors using ZnO as an active channel layer and their electrical properties, J. Appl. Phys. 93 (3) (2003) 1624–1630.
[5] S. Gieraltowska, L. Wachnicki, B.S. Witkowski, E. Guziewicz, M. Godlewski, Thin films of high-k oxides and ZnO for transparent electronic devices, Chem. Vap. Depos. 19 (4–6) (2013) 213–220.
[6] R.L. Hoffman, B.J. Norris, J.F. Wager, ZnO-based transparent thin-film transistors, Appl. Phys. Lett. 82 (5) (2003) 733–735.
[7] M.H. Hsu, C.J. Chang, S-Doped ZnO nanorods on stainless-steel wire mesh as immobilized hierarchical photocatalysts for photocatalytic H2 production, Int. J. Hydrogen Energy 39 (29) (2014) 16524–16533.
[8] X. Lu, G. Wang, S. Xie, J. Shi, W. Li, Y. Tong, Y. Li, Efficient photocatalytic hydrogen evolution over hydrogenated ZnO nanorod arrays, Chem. Commun. 48 (62) (2012) 7717.
[9] H. Kim, K. Yong, Highly efficient photoelectrochemical hydrogen generation using a quantum dot coupled hierarchical ZnO nanowires array, Appl. Mater. Interf. (2013).
[10] M. Weber, A. Julbe, A. Ayral, P. Miele, M. Bechelany, Atomic layer deposition for membranes: basics, challenges and opportunities, Chem. Mater. (2018) acs.chemmater.8b02687.
[11] Ü. Özgür, Ya.I. Alivov, C. Liu, A. Teke, M.A. Reshchikov, S. Doğan, V. A., S.-J. Cho, H. M., A comprehensive review of ZnO materials and devices, J. Appl. Phys. 98 (4) (2005) 1–103.
[12] O. Graniel, M. Weber, S. Balme, P. Miele, M. Bechelany, Atomic layer deposition for biosensing applications, Biosens. Bioelectron. 122 (September) (2018) 147–159.
[13] M. Baitimirova, R. Viter, J. Andzane, A. Van Der Lee, D. Voiry, I. Iatsunskyi, E. Coy, L. Mikoliunaite, S. Tumenas, K. Zaleski, et al., Tuning of structural and optical properties of graphene/ZnO nanolaminates, J. Phys. Chem. C 120 (41) (2016) 23716–23725.

[14] E. Przeździecka, Ł. Wachnicki, W. Paszkowicz, E. Łusakowska, T. Krajewski, G. Łuka, E. Guziewicz, M. Godlewski, Photoluminescence, electrical and structural properties of ZnO films, grown by ALD at low temperature, Semicond. Sci. Technol. 24 (10) (2009) 105014.
[15] T. Tynell, M. Karppinen, Atomic layer deposition of ZnO: a review, Semicond. Sci. Technol. 29 (4) (2014) 043001.
[16] A. Rahtu, T. Alaranta, M. Ritala, In situ quartz crystal microbalance and quadrupole mass spectrometry studies of atomic layer deposition of aluminum oxide from trimethylaluminum and water, Langmuir 17 (21) (2001) 6506–6509.
[17] A. Yanguas-Gil, J.A. Libera, J.W. Elam, Modulation of the growth per cycle in atomic layer deposition using reversible surface functionalization, Chem. Mater. 25 (24) (2013) 4849–4860.
[18] R.L. Puurunen, Surface chemistry of atomic layer deposition: a case study for the trimethylaluminum/water process, J. Appl. Phys. 97 (12) (2005).
[19] E.B. Yousfi, J. Fouache, D. Lincot, Study of atomic layer epitaxy of zinc oxide by in-situ quartz crystal microgravimetry, Appl. Surf. Sci. 153 (4) (2000) 223–234.
[20] A. Afshar, K.C. Cadien, Growth mechanism of atomic layer deposition of zinc oxide: a density functional theory approach, Appl. Phys. Lett. 103 (2013) (25).
[21] T. Weckman, K. Laasonen, Atomic layer deposition of zinc oxide: study on the water pulse reactions from first-principles, J. Phys. Chem. C 122 (2018) 7685–7694.
[22] J. Ren, Initial growth mechanism of atomic layer deposition of ZnO on the hydroxylated Si(1 0 0)-2x1: a density functional theory study, Appl. Surf. Sci. 255 (11) (2009) 5742–5745.
[23] T. Weckman, K. Laasonen, Atomic layer deposition of zinc oxide: diethyl zinc reactions and surface saturation from first-principles, J. Phys. Chem. C 120 (38) (2016) 21460–21471.
[24] R.L. Puurunen, Growth per cycle in atomic layer deposition: a theoretical model, Chem. Vap. Depos. 9 (5) (2003) 249–257.
[25] J.D. Ferguson, A.W. Weimer, S.M. George, Surface chemistry and infrared absorbance changes during ZnO atomic layer deposition on ZrO2 and BaTiO3 particles, J. Vac. Sci. Technol. A Vacuum, Surf., Film 23 (1) (2005) 118–125.
[26] R.L. Puurunen, Growth per cycle in atomic layer deposition: real application examplesof a theoretical model, Chem. Vap. Depos. 9 (6) (2003) 327–332.
[27] T. Törndahl, C. Platzer-Björkman, J. Kessler, M. E., Atomic layer deposition of Zn(1-x)MgxO buffer layers for Cu(In,Ga)Se2 solar cells. Prog. Photovolt. Res. Appl. 15 (February 2013) (2007) 659–676.
[28] K. Morishige, S. Kittaka, T. Moriyasu, T. Morimoto, Thermal desorption study of surface hydroxyls on ZnO, J. Chem. Soc. Faraday Trans. 1 (76) (1980) 728–745.
[29] J. Provine, P. Schindler, J. Torgersen, H.J. Kim, H.-P. Karnthaler, F.B. Prinz, Atomic layer deposition by reaction of molecular oxygen with tetrakisdimethylamido-metal precursors, J. Vac. Sci. Technol. A Vacuum, Surf., Film. 34 (1) (2016) 01A138.
[30] A. Holmqvist, T. Törndahl, F. Magnusson, U. Zimmermann, S. Stenström, Dynamic parameter estimation of atomic layer deposition kinetics applied to in situ quartz crystal microbalance diagnostics, Chem. Eng. Sci. 111 (2014) 15–33.
[31] H. Makino, A. Miyake, T. Yamada, N. Yamamoto, T. Yamamoto, Influence of substrate temperature and Zn-precursors on atomic layer deposition of polycrystalline ZnO films on glass, Thin Solid Films 517 (10) (2009) 3138–3142.
[32] V. Lujala, J. Skarp, M. Tammenmaa, T. Suntola, Atomic layer epitaxy growth of doped zinc oxide thin films from organometals, Appl. Surf. Sci. 82–83(C) (1994) 34–40.